PHYSICAL REVIEW D **95,** 012006 (2017)

Observation of the decay $B_s^0 \to \phi\pi^+\pi^-$ and evidence for $B^0 \to \phi\pi^+\pi^-$

R. Aaij *et al.*[*]
(LHCb Collaboration)

(Received 19 October 2016; published 10 January 2017)

The first observation of the rare decay $B_s^0 \to \phi\pi^+\pi^-$ and evidence for $B^0 \to \phi\pi^+\pi^-$ are reported, using pp collision data recorded by the LHCb detector at center-of-mass energies $\sqrt{s} = 7$ and 8 TeV, corresponding to an integrated luminosity of 3 fb^{-1}. The branching fractions in the $\pi^+\pi^-$ invariant mass range $400 < m(\pi^+\pi^-) < 1600$ MeV/c^2 are $[3.48 \pm 0.23 \pm 0.17 \pm 0.35] \times 10^{-6}$ and $[1.82 \pm 0.25 \pm 0.41 \pm 0.14] \times 10^{-7}$ for $B_s^0 \to \phi\pi^+\pi^-$ and $B^0 \to \phi\pi^+\pi^-$ respectively, where the uncertainties are statistical, systematic and from the normalization mode $B_s^0 \to \phi\phi$. A combined analysis of the $\pi^+\pi^-$ mass spectrum and the decay angles of the final-state particles identifies the exclusive decays $B_s^0 \to \phi f_0(980)$, $B_s^0 \to \phi f_2(1270)$, and $B_s^0 \to \phi\rho^0$ with branching fractions of $[1.12 \pm 0.16^{+0.09}_{-0.08} \pm 0.11] \times 10^{-6}$, $[0.61 \pm 0.13^{+0.12}_{-0.05} \pm 0.06] \times 10^{-6}$ and $[2.7 \pm 0.7 \pm 0.2 \pm 0.2] \times 10^{-7}$, respectively.

DOI: 10.1103/PhysRevD.95.012006

I. INTRODUCTION

The decays $B_s^0 \to \phi\pi^+\pi^-$ and $B^0 \to \phi\pi^+\pi^-$ have not been observed before. They are examples of decays that are dominated by contributions from flavor changing neutral currents (FCNC), which provide a sensitive probe for the effect of physics beyond the Standard Model because their amplitudes are described by loop (or penguin) diagrams where new particles may enter [1]. A well-known example of this type of decay is $B_s^0 \to \phi\phi$ which has a branching fraction of 1.9×10^{-5} [2]. First measurements of the CP-violating phase ϕ_s in this mode have recently been made by the LHCb Collaboration [3,4]. The decay $B_s^0 \to \phi f_0(980)$ also proceeds via a gluonic $b \to s$ penguin transition [see Fig. 1(a)], with an expected branching fraction of approximately 2×10^{-6}, based on the ratio of the $B_s^0 \to J/\psi f_0(980)$ and $B_s^0 \to J/\psi\phi$ decays [2]. When large statistics samples are available, similar time-dependent CP violation studies will be possible with $B_s^0 \to \phi f_0(980)$.

The decay $B_s^0 \to \phi\rho^0$ is of particular interest,[1] because it is an isospin-violating $\Delta I = 1$ transition which is mediated by a combination of an electroweak penguin diagram and a suppressed $b \to u$ transition [see Fig. 1(b)]. The predicted branching fraction is $[4.4^{+2.2}_{-0.7}] \times 10^{-7}$, and large CP-violating asymmetries are not excluded [5].

The corresponding B^0 decays are mediated by CKM-suppressed $b \to d$ penguin diagrams, and are expected to have branching fractions an order of magnitude lower than the B_s^0 decays. The *BABAR* experiment has set an upper limit on the branching fraction of the decay $B^0 \to \phi\rho^0$ of 3.3×10^{-7} at 90% confidence level [6].

This paper reports a time-integrated and flavor-untagged search, using a data set with an integrated luminosity of approximately 3 fb^{-1} collected by the LHCb detector in 2011 and 2012 at center-of-mass energies of $\sqrt{s} = 7$ and 8 TeV, respectively. This leads to the first observation of $B_s^0 \to \phi\pi^+\pi^-$ decays, and evidence for $B^0 \to \phi\pi^+\pi^-$ decays, with the $\pi^+\pi^-$ invariant mass in the range $400 < m(\pi^+\pi^-) < 1600$ MeV/c^2. A combined angular and $\pi^+\pi^-$ mass analysis of the $B_s^0 \to \phi\pi^+\pi^-$ sample identifies contributions from the exclusive decays $B_s^0 \to \phi f_0(980)$, $B_s^0 \to \phi f_2(1270)$, and $B_s^0 \to \phi\rho^0$. There is also a significant S-wave $\pi^+\pi^-$ contribution in the high-mass region $1350 < m(\pi^+\pi^-) < 1600$ MeV/c^2.

The branching fractions for both the inclusive and exclusive decays are determined with respect to the normalization mode $B_s^0 \to \phi\phi$. This mode has a very similar topology and a larger branching fraction, which has been measured by the LHCb Collaboration [7] to be $\mathcal{B}(B_s^0 \to \phi\phi) = [1.84 \pm 0.05 \pm 0.07 \pm 0.11 \pm 0.12] \times 10^{-5}$, where the uncertainties are respectively statistical, systematic, from the fragmentation function f_s/f_d giving the ratio of B_s^0 to B^0 production at the LHC, and from the measurement of the branching fraction of $B^0 \to \phi K^{*0}$ at the B factories [8,9].

II. DETECTOR AND SOFTWARE

The LHCb detector [10,11] is a single-arm forward spectrometer covering the pseudorapidity range $2 < \eta < 5$. It is designed for the study of particles containing b or c

[1]Unless otherwise stated, ρ^0 represents the $\rho(770)^0$, K^{*0} represents the $K^*(892)^0$, ϕ represents the $\phi(1020)$, and charge-conjugate decays are implied throughout this paper.

[*]Full author list given at the end of the article.

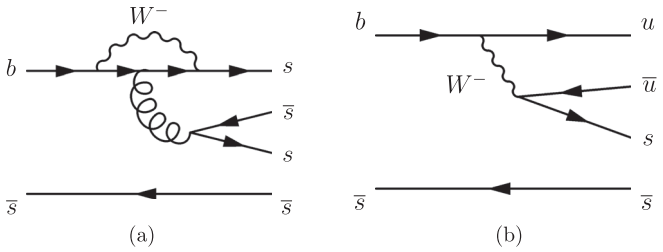

FIG. 1. Feynman diagrams for the exclusive decays (a) $B_s^0 \to \phi f_0(980)$ and (b) $B_s^0 \to \phi\rho^0$.

quarks, which are produced preferentially as pairs at small angles with respect to the beam axis. The detector includes a high-precision tracking system consisting of a silicon-strip vertex detector surrounding the pp interaction region, a large-area silicon-strip tracker located upstream of a dipole magnet with a bending power of about 4 Tm, and three stations of silicon-strip trackers and straw drift tubes placed downstream of the magnet. The tracking system provides a measurement of charged particle momenta with a relative uncertainty that varies from 0.5% at 5 GeV/c to 1.0% at 200 GeV/c. The minimum distance of a track to a primary pp interaction vertex (PV), the impact parameter (IP), is measured with a resolution of $(15 + 29/p_{\mathrm{T}})$ μm, where p_{T} is the component of the momentum transverse to the beam, in GeV/c. Different types of charged hadrons are distinguished using information from two ring-imaging Cherenkov detectors. Photon, electron, and hadron candidates are identified by a calorimeter system consisting of scintillating-pad and preshower detectors, an electromagnetic calorimeter and a hadronic calorimeter. Muons are identified by a system composed of alternating layers of iron and multiwire proportional chambers.

The trigger [12] consists of a hardware stage, based on information from the calorimeter and muon systems, followed by a software stage, which applies a full event reconstruction. The software trigger requires a two-, three- or four-track secondary vertex with a significant displacement from an associated PV. At least one charged particle must have a transverse momentum $p_{\mathrm{T}} > 1.7$ GeV/c and be inconsistent with originating from the PV. A multivariate algorithm [13] is used for the identification of secondary vertices consistent with the decay of a b hadron into charged hadrons. In addition, an algorithm is used that identifies inclusive $\phi \to K^+K^-$ production at a secondary vertex, without requiring a decay consistent with a b hadron.

In the simulation, pp collisions are generated using Pythia 6 [14] with a specific LHCb configuration [15]. Decays of hadronic particles are described by EvtGen [16], in which final-state radiation is generated using Photos [17]. The interaction of the generated particles with the detector and its response are implemented using the Geant4 toolkit [18] as described in Ref. [19].

III. SELECTION

The offline selection of candidates consists of two parts. First, a selection with loose criteria is performed that reduces the combinatorial background as well as removing some specific backgrounds from other exclusive b-hadron decay modes. In a second stage a multivariate method is applied to further reduce the combinatorial background and improve the signal significance.

The selection starts from well-reconstructed particles that traverse the entire spectrometer and have $p_T > 500$ MeV/c. Spurious tracks created by the reconstruction are suppressed using a neural network trained to discriminate between these and real particles. A large track IP with respect to any PV is required, consistent with the track coming from a displaced secondary decay vertex. The information provided by the ring-imaging Cherenkov detectors is combined with information from the tracking system to select charged particles consistent with being a kaon, pion or proton. Tracks that are identified as muons are removed at this stage.

Pairs of oppositely charged kaons that originate from a common vertex are combined to form a ϕ meson candidate. The transverse momentum of the ϕ meson is required to be larger than 0.9 GeV/c and the invariant mass to be within 10 MeV/c^2 of the known value [2]. Similarly, pairs of oppositely charged pions are combined if they form a common vertex and if the transverse momentum of the $\pi^+\pi^-$ system is larger than 1 GeV/c. For this analysis, the invariant mass of the pion pair is required to be in the range $400 < m(\pi^+\pi^-) < 1600$ MeV/c^2, below the charm threshold. The ϕ candidates and $\pi^+\pi^-$ pairs are combined to form B^0 or B_s^0 meson candidates. To further reject combinatorial background, the reconstructed flight path of the B candidates must be consistent with coming from a PV.

There are several decays of b hadrons proceeding via charmed hadrons that need to be explicitly removed. The decay modes $B_s^0 \to D_s^-\pi^+$ and $B^0 \to D^-\pi^+$ are rejected when the invariant mass of the $K^+K^-\pi^-$ system is within 3 standard deviations (σ) of either D meson mass. The decay mode $\overset{(-)}{B} \to \overset{(-)}{D} K^\pm\pi^\mp$ is rejected when the invariant mass of either of the $K^\pm\pi^\mp$ combinations is within 2σ of the D^0 mass. Backgrounds from D^- decays to $K^+\pi^-\pi^-$ and from Λ_c^+ decays to $pK^-\pi^+$ are removed if the three-body invariant mass, calculated assuming that either a π^- or a proton has been misidentified as a kaon, is within 3σ of the charm hadron mass.

Another background arises from the decay $B^0 \to \phi K^{*0}$, where the kaon from the decay $K^{*0} \to K^+\pi^-$ is misidentified as a pion. To remove it, the invariant masses $m(K^+\pi^-)$ and $m(K^+K^-K^+\pi^-)$ are calculated assuming that one of the K^+ has been misidentified as a π^+, and candidates are rejected if $m(K^+\pi^-)$ is within 3 decay widths of the K^{*0}, and $m(K^+K^-K^+\pi^-)$ is consistent with the B^0 mass to

within 3 times the experimental resolution. The higher resonance mode $B^0 \to \phi K_2^{*0}(1430)$ is vetoed in a similar fashion. The efficiency of the charm and ϕK^{*0} vetoes is 94%, evaluated on the $B_s^0 \to \phi\pi^+\pi^-$ simulation sample, with the ϕK^{*0} veto being 99% efficient. For the decay $B^0 \to \phi\pi^+\pi^-$ this efficiency is reduced to 84% by the larger impact of the ϕK^{*0} veto.

In the second stage of the selection a boosted decision tree (BDT) [20,21] is employed to further reduce the combinatorial background. This makes use of twelve variables related to the kinematics of the B meson candidate and its decay products, particle identification for the kaon candidates and the B decay vertex displacement from the PV. It is trained using half of both the simulated signal sample and the background events from the data in the range $5450 < m(K^+K^-\pi^+\pi^-) < 5600$ MeV$/c^2$, and validated using the other half of each sample. For a signal efficiency of 90% the BDT has a background rejection of 99%.

A sample of $B_s^0 \to \phi\phi$ candidates has been selected using the same methods as for the signal modes, apart from the particle identification criteria and the $m(K^+K^-)$ mass window for the second ϕ meson, and without the ϕK^{*0} veto. The BDT deliberately does not include particle identification for the pion candidates, because this part of the selection is different between the signal mode and the $B_s^0 \to \phi\phi$ normalization mode.

For the signal mode a tighter selection is made on the pion identification as part of a two-dimensional optimization together with the BDT output. The figure of merit (FOM) used to maximize the discovery potential for a new signal is [22],

$$\text{FOM} = \frac{\varepsilon_S}{5/2 + \sqrt{B}},$$

where ε_S is the signal efficiency evaluated using the simulation and B is the number of background candidates expected within a 50 MeV$/c^2$ window about the B_s^0 mass. The optimized selection on the BDT output and the pion identification has a signal efficiency $\varepsilon_S = 0.846$.

IV. INVARIANT MASS FIT

The yields for the inclusive $B_s^0 \to \phi\pi^+\pi^-$ and $B^0 \to \phi\pi^+\pi^-$ signals are determined from a fit to the invariant $K^+K^-\pi^+\pi^-$ mass distribution of selected candidates in the range $5100 < m(K^+K^-\pi^+\pi^-) < 5600$ MeV$/c^2$. The fit includes possible signal contributions from both B_s^0 and B^0 decays, as well as combinatorial background. Backgrounds from partially reconstructed decays such as $B_s^0 \to \phi\phi(\to \pi^+\pi^-\pi^0)$ and $B_s^0 \to \phi\eta'(\to \pi^+\pi^-\gamma)$ are negligible in the region $m(K^+K^-\pi^+\pi^-) > 5100$ MeV$/c^2$. After the veto the contribution from $B^0 \to \phi K^{*0}$ can also be neglected.

The line shapes for the $B_s^0 \to \phi\pi^+\pi^-$ signal and $B_s^0 \to \phi\phi$ normalization mode are determined using simulated events, and parametrized by a sum of two Gaussian functions with a common mean and different widths. In the fits to data the means and widths of the narrow Gaussians for the B_s^0 modes are fitted, but the relative widths and fractions of the broader Gaussians relative to the narrow ones are taken from the simulation. The mean and width of the B^0 signal shape are scaled down from $B_s^0 \to \phi\pi^+\pi^-$ to account for the mass difference [2], and to correct for a slight modification of the B^0 shape due to the ϕK^{*0} veto. The combinatorial background is modeled by an exponential function with a slope that is a free parameter in the fit to the data.

Figure 2 shows the result of the extended unbinned maximum likelihood fit to the $m(K^+K^-\pi^+\pi^-)$ distribution. There is clear evidence for both $B_s^0 \to \phi\pi^+\pi^-$ and $B^0 \to \phi\pi^+\pi^-$ signals. The B_s^0 and B^0 yields are 697 ± 30 and 131 ± 17 events, respectively, and the fit has a chi-squared per degree of freedom, χ^2/ndf, of 0.87. Figure 3 shows the $m(K^+K^-K^+K^-)$ distribution for the $B_s^0 \to \phi\phi$ normalization mode, with a fit using a sum of two Gaussians for the B_s^0 signal shape. There are 2424 ± 51 events above a very low combinatorial background. Backgrounds from other decay modes are negligible with this selection.

To study the properties of the $B_s^0 \to \phi\pi^+\pi^-$ signal events, the combinatorial background and B^0 contribution are subtracted using the *sPlot* method [23]. The results of the invariant mass fit are used to assign to each event a signal weight that factorizes out the signal part of the sample from the other contributions. These weights can then be used to project out other kinematic properties of the signal, provided that these properties are uncorrelated with $m(K^+K^-\pi^+\pi^-)$. In the next section the decay angle and $m(\pi^+\pi^-)$ distributions of the $B_s^0 \to \phi\pi^+\pi^-$ signal events

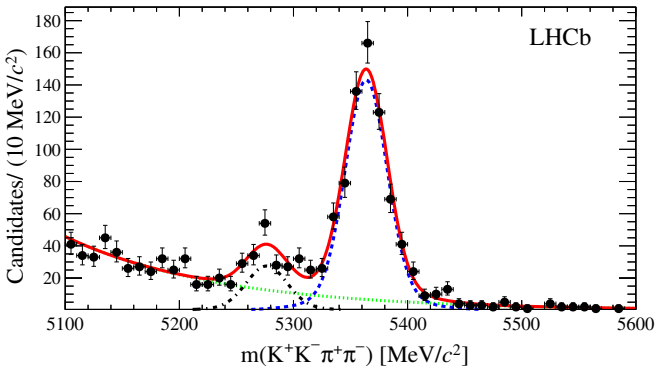

FIG. 2. The $K^+K^-\pi^+\pi^-$ invariant mass distribution for candidates in the mass range $0.4 < m_{\pi\pi} < 1.6$ GeV$/c^2$. The fit described in the text is overlaid. The solid (red) line is the total fitted function, the dotted (green) line the combinatorial background, the dashed (blue) line the B_s^0 and the dot-dashed (black) line the B^0 signal component.

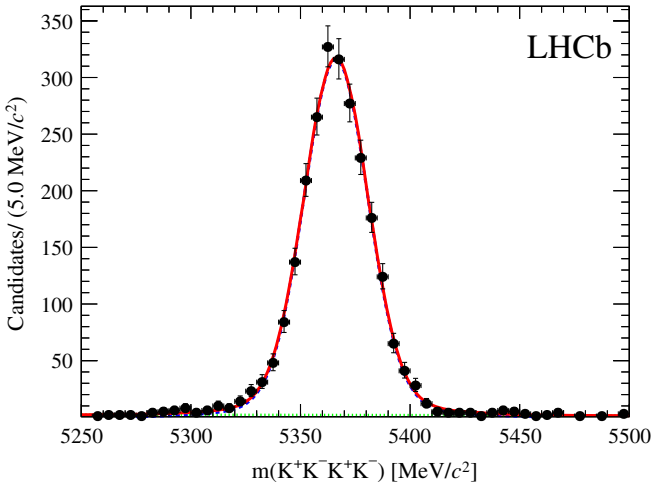

FIG. 3. The $K^+K^-K^+K^-$ invariant mass distribution after all selection criteria. The solid (red) line is the total fitted function including the $B_s^0 \to \phi\phi$ signal, and the dashed (green) line is the combinatorial background.

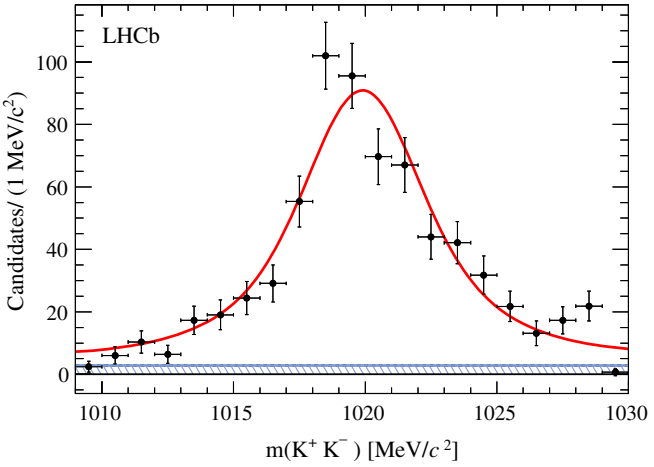

FIG. 4. The K^+K^- invariant mass distribution for background-subtracted $B_s^0 \to \phi\pi^+\pi^-$ signal events with a fit to the dominant P-wave ϕ meson shown as a solid (red) line, and a small S-wave K^+K^- contribution shown as a hatched (blue) area.

are used to study the resonant $\pi^+\pi^-$ contributions. Figure 4 shows the K^+K^- invariant mass distribution for the $B_s^0 \to \phi\pi^+\pi^-$ signal, which is consistent with a dominant ϕ meson resonance together with a small contribution from a nonresonant S-wave K^+K^- component. The ϕ contribution is modeled by a relativistic Breit-Wigner function, whose natural width is convolved with the experimental K^+K^- mass resolution, and the S-wave component is modeled by a linear function. The S-wave K^+K^- component is fitted to be $(8.5 \pm 3.8)\%$ of the signal yield in a ± 10 MeV$/c^2$ window around the known ϕ mass. A similar fit to the $B_s^0 \to \phi\phi$ normalization mode gives an S-wave component of $(1.4 \pm 1.1)\%$.

V. AMPLITUDE ANALYSIS

There are several resonances that can decay into a $\pi^+\pi^-$ final state in the region $400 < m(\pi^+\pi^-) < 1600$ MeV$/c^2$. These are listed in Table I together with the mass models used to describe them and the source of the model parameters.[2] To study the resonant contributions, an amplitude analysis is performed using an unbinned maximum likelihood fit to the $m(\pi^+\pi^-)$ mass and decay angle distributions of the B_s^0 candidates with their signal weights obtained by the *sPlot* technique. In the fit the uncertainties on the signal weights are taken into account in determining the uncertainties on the fitted amplitudes and phases.

Three decay angles are defined in the transversity basis as illustrated in Fig. 5, where θ_1 is the $\pi^+\pi^-$ helicity angle between the π^+ direction in the $\pi^+\pi^-$ rest frame and the $\pi^+\pi^-$ direction in the B rest frame, θ_2 is the K^+K^- helicity angle between the K^+ direction in the ϕ rest frame and the ϕ direction in the B rest frame, and Φ is the acoplanarity angle between the $\pi^+\pi^-$ system and the ϕ meson decay planes.

The LHCb detector geometry and the kinematic selections on the final state particles lead to detection efficiencies that vary as a function of $m(\pi^+\pi^-)$ and the decay angles. This is studied using simulated signal events, and is parametrized by a four-dimensional function using Legendre polynomials, taking into account the correlations between the variables. Figure 6 shows the projections of the detection efficiency and the function used to describe it. There is a significant drop of efficiency at $\cos\theta_1 = \pm 1$, a smaller reduction of efficiency for $\cos\theta_2 = \pm 1$, a flat efficiency in Φ, and a monotonic efficiency increase with

TABLE I. Possible resonances contributing to the $m(\pi^+\pi^-)$ mass distribution. The shapes are either relativistic Breit-Wigner (BW) functions, or empirical threshold functions for the $f_0(500)$ proposed by Bugg [25] based on data from BES, and for the $f_0(980)$ proposed by Flatté [26] to account for the effect of the K^+K^- threshold.

Resonance	Spin	Shape	Mass	Width	Source
$f_0(500)$	0	Bugg	400–800	Broad	BES [25]
ρ^0	1	BW	775	149	PDG [2]
$f_0(980)$	0	Flatté	980	40–100	LHCb [27]
$f_2(1270)$	2	BW	1275	185	PDG [2]
$f_0(1370)$	0	BW	1200–1500	200–500	PDG [2]
$f_2(1430)$	2	BW	1421	30	DM2 [28]
$\rho(1450)$	1	BW	1465	400	PDG [2]
$f_0(1500)$	0	BW	1461	124	LHCb [29]

[2]Note that the description of the broad $f_0(1370)$ and $f_0(1500)$ resonances by Breit-Wigner functions is known not to be a good approximation when they both make significant contributions [24].

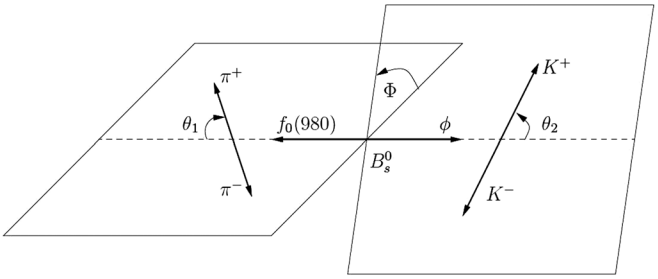

FIG. 5. The definition of the decay angles θ_1, θ_2, and Φ for the decay $B_s^0 \to \phi\pi^+\pi^-$ with $\phi \to K^+K^-$ and taking $f_0(980) \to \pi^+\pi^-$ for illustration.

$m(\pi^+\pi^-)$. This efficiency dependence is included in the amplitude fits.

The decay rate for the mass range $m(\pi^+\pi^-) < 1100\ \mathrm{MeV}/c^2$ can be described primarily by the S-wave and P-wave $\pi^+\pi^-$ contributions from the $f_0(980)$ and ρ^0 mesons. The S-wave contribution is parametrized by a single amplitude A_S. For the P-wave there are three separate amplitudes A_0, $A_\perp$ and $A_\parallel$ from the possible spin configurations of the final state vector mesons. The amplitudes A_j, where $j = (0, \perp, \parallel, S)$, are complex and can be written as $|A_j|e^{i\delta_j}$. By convention, the phase δ_S is chosen to be zero. In the region $m(\pi^+\pi^-) > 1100\ \mathrm{MeV}/c^2$ the differential decay rate requires additional contributions from the D-wave $f_2(1270)$ meson and other possible resonances at higher mass.

The total differential decay rate is given by the square of the sum of the amplitudes. It can be written as

$$\frac{d^4\Gamma}{d\cos\theta_1 d\cos\theta_2 d\Phi dm_{\pi\pi}} = \frac{9}{8\pi}\sum_i T_i f_i(\theta_1, \theta_2, \Phi)\mathcal{M}_i(m_{\pi\pi})d\Omega_4(KK\pi\pi), \quad (1)$$

where the T_i are either squares of the amplitudes A_j or interference terms between them, f_i are decay angle distributions, $\mathcal{M}_i$ are resonant $\pi^+\pi^-$ mass distributions and $d\Omega_4$ is the phase-space element for four-body decays. The detailed forms of these functions are given in Table II for the contributions from the $f_0(980)$, ρ^0 and $f_2(1270)$ resonances. Note that interference terms between CP-even

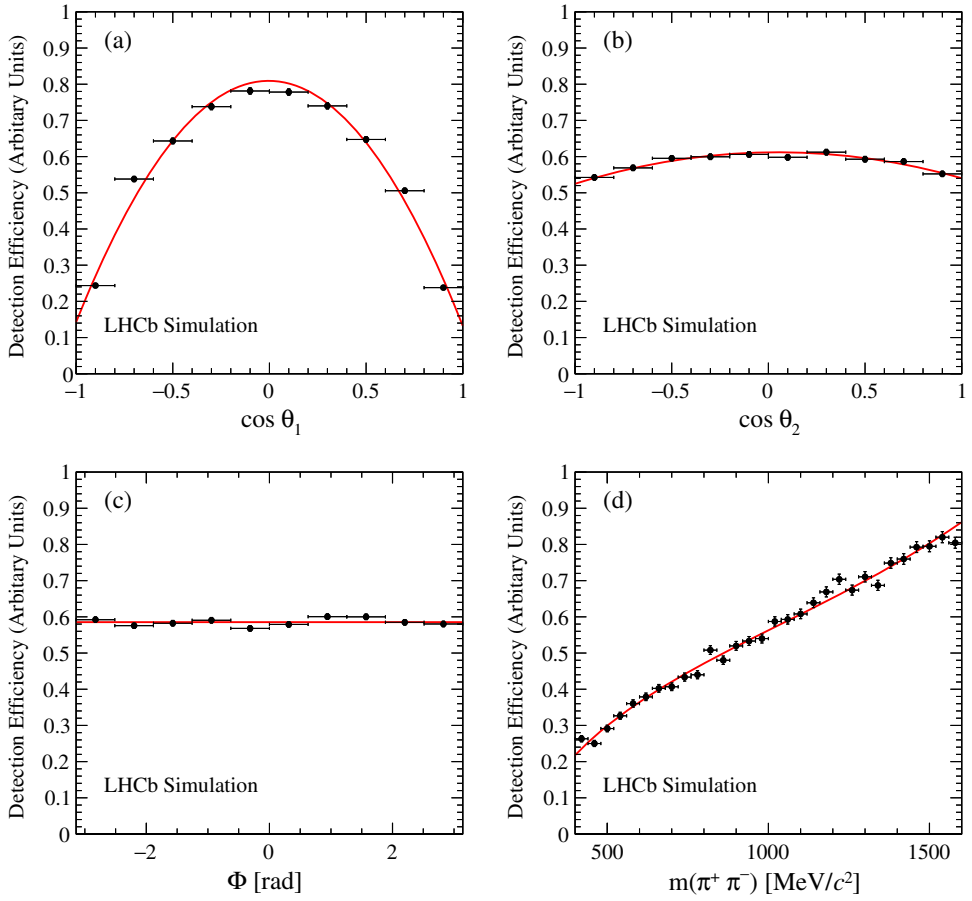

FIG. 6. One-dimensional projections of the detection efficiency parametrized using Legendre polynomials (solid red lines) as a function of (a) $\cos\theta_1$, (b) $\cos\theta_2$, (c) Φ and (d) $m(\pi^+\pi^-)$, superimposed on the efficiency determined from the ratio of the accepted/generated $B_s^0 \to \phi\pi^+\pi^-$ events.

TABLE II. The individual terms $i = 1$ to $i = 6$ come from the S-wave and P-wave $\pi^+\pi^-$ amplitudes associated with the $f_0(980)$ and ρ^0, and the terms $i = 7$ to $i = 12$ come from the D-wave amplitudes associated with the $f_2(1270)$. See the text for definitions of T_i, f_i and $\mathcal{M}_i$, and for a discussion of the interference terms omitted from this table.

i	T_i	$f_i\,(\theta_1, \theta_2, \Phi)$	$\mathcal{M}_i(m_{\pi\pi})$
1	$\lvert A_0\rvert^2$	$\cos^2\theta_1\cos^2\theta_2$	$\lvert M_1(m_{\pi\pi})\rvert^2$
2	$\lvert A_\parallel\rvert^2$	$\frac{1}{4}\sin^2\theta_1\sin^2\theta_2(1+\cos 2\Phi)$	$\lvert M_1(m_{\pi\pi})\rvert^2$
3	$\lvert A_\perp\rvert^2$	$\frac{1}{4}\sin^2\theta_1\sin^2\theta_2(1-\cos 2\Phi)$	$\lvert M_1(m_{\pi\pi})\rvert^2$
4	$\lvert A_\parallel A_0^*\rvert$	$\sqrt{2}\cos\theta_1\sin\theta_1\cos\theta_2\sin\theta_2\cos\Phi$	$\lvert M_1(m_{\pi\pi})\rvert^2\cos(\delta_\parallel-\delta_0)$
5	$\lvert A_S\rvert^2$	$\frac{1}{3}\cos^2\theta_2$	$\lvert M_0(m_{\pi\pi})\rvert^2$
6	$\lvert A_\perp A_S^*\rvert$	$\frac{\sqrt{6}}{3}\sin\theta_1\cos\theta_2\sin\theta_2\sin\Phi$	$\mathcal{R}e[M_1(m_{\pi\pi})M_0^*(m_{\pi\pi})e^{i\delta_\perp}]$
7	$\lvert A_0^{1270}\rvert^2$	$\frac{5}{12}(3\cos^2\theta_1-1)^2\cos^2\theta_2$	$\lvert M_2(m_{\pi\pi})\rvert^2$
8	$\lvert A_\parallel^{1270}\rvert^2$	$\frac{5}{2}\sin^2\theta_1\sin^2\theta_2\cos^2\theta_1\cos^2\Phi$	$\lvert M_2(m_{\pi\pi})\rvert^2$
9	$\lvert A_\perp^{1270}\rvert^2$	$\frac{5}{2}\sin^2\theta_1\sin^2\theta_2\cos^2\theta_1\sin^2\Phi$	$\lvert M_2(m_{\pi\pi})\rvert^2$
10	$\lvert A_\parallel^{1270}A_0^{1270*}\rvert$	$\frac{5}{4\sqrt{6}}(3\cos^2\theta_1-1)\sin 2\theta_1\sin 2\theta_2\cos\Phi$	$\lvert M_2(m_{\pi\pi})\rvert^2\cos(\delta_\parallel^{1270}-\delta_0^{1270})$
11	$\lvert A_\parallel^{1270}A_S^*\rvert$	$\frac{\sqrt{10}}{3}\sin\theta_1\cos\theta_1\sin\theta_2\cos\theta_2\cos\Phi$	$\mathcal{R}e\left[M_2(m_{\pi\pi})M_0^*(m_{\pi\pi})e^{i\delta_\parallel^{1270}}\right]$
12	$\lvert A_0^{1270}A_S^*\rvert$	$\frac{\sqrt{5}}{3}(3\cos^2\theta_1-1)\cos^2\theta_2$	$\mathcal{R}e\left[M_2(m_{\pi\pi})M_0^*(m_{\pi\pi})e^{-i\delta_0^{1270}}\right]$

amplitudes (A_0, $A_\parallel$, $A_\perp^{1270}$) and CP-odd amplitudes (A_S, $A_\perp$, A_0^{1270}, $A_\parallel^{1270}$) can be ignored in the sum of B_s^0 and $\bar{B}_s^0$ decays in the absence of CP violation, as indicated by the measurements in the related decay $B_s^0 \to \phi\phi$ [4]. With this assumption one CP-even phase $\delta_\perp^{1270}$ can also be chosen to be zero. The fit neglects the interference terms between P- and D-waves, and the P-wave-only interference term ($i = 4$ in Table II), which are all found to be small when included in the fit. This leaves only a single P-wave phase $\delta_\perp$ and two D-wave phases $\delta_\parallel^{1270}$ and δ_0^{1270} to be fitted for these three resonant contributions.

Several amplitude fits have been performed including different resonant contributions. All fits include the $f_0(980)$ and $f_2(1270)$ resonances. The high-mass region $1350 < m(\pi^+\pi^-) < 1600$ MeV/c^2 has been modeled by either an S-wave or a D-wave $\pi^+\pi^-$ contribution, where the masses and widths of these contributions are determined by the fits, but the shapes are constrained to be Breit-Wigner functions. In each case the respective terms in Table II from $f_0(980)$ or $f_2(1270)$ have to be duplicated for the higher resonance. For the higher S-wave contribution this introduces one new amplitude A_S^{1500} and phase δ_S^{1500}, and there is an additional interference term between the two S-wave resonances. For the higher D-wave contribution $f_2(1430)$ there are three new amplitudes and phases, and several interference terms between the two D-wave resonances. A contribution from the P-wave $\rho(1450)$ has also been considered, but is found to be negligible and is not included in the final fit. The fit quality has been assessed using a binned χ^2 calculation based on the projected $\cos\theta_1$, $\cos\theta_2$ and $m(\pi^+\pi^-)$ distributions. In the high-mass region the best fit uses an S-wave component with a fitted mass and width of 1427 ± 7 MeV/c^2 and 143 ± 17 MeV/c^2, hereafter referred to as the $f_0(1500)$ for convenience. The mass is lower than the accepted value of 1504 ± 6 MeV/c^2 for the $f_0(1500)$[2]. It is also lower than the equivalent S-wave component in $B_s^0 \to J/\psi\pi^+\pi^-$ where the fitted mass and width were 1461 ± 3 MeV/c^2 and 124 ± 7 MeV/c^2 [29]. This may be due to the absence of contributions from the ρ^0 and $f_2(1270)$ in $B_s^0 \to J/\psi\pi^+\pi^-$. It has been suggested [24,30] that the observed $m(\pi^+\pi^-)$ distributions can be described by an interference between the $f_0(1370)$ and $f_0(1500)$, but with the current statistics of the $B_s^0 \to \phi\pi^+\pi^-$ sample it is not possible to verify this.

In the low-mass region $m(\pi^+\pi^-) < 900$ MeV/c^2 the effect of adding a contribution from the ρ^0 is studied. The ρ^0 contribution significantly improves the fit quality and has a statistical significance of 4.5σ, estimated by running pseudoexperiments. A contribution from the $f_0(500)$ has been considered as part of the systematics. The preferred fit, including the ρ^0, $f_0(980)$, $f_2(1270)$ and $f_0(1500)$, has $\chi^2/\text{ndf} = 34/20$. Removing the ρ^0 increases this to $\chi^2/\text{ndf} = 53/24$, and replacing the S-wave $f_0(1500)$ with a D-wave $f_2(1430)$ increases it to $\chi^2/\text{ndf} = 78/16$. The projections of the preferred fit, including the ρ^0, $f_0(980)$, $f_2(1270)$ and $f_0(1500)$, are shown in Fig. 7. The fitted amplitudes and phases are given in Table III. From Fig. 7 it can be seen that the low numbers of observed candidates in the regions $|\cos\theta_1| > 0.8$ and $|\cos\theta_2| < 0.4$ require a large S-wave $\pi^+\pi^-$ contribution, and smaller P-wave and D-wave contributions.

To convert the fitted amplitudes into fractional contributions from different resonances they need to be first

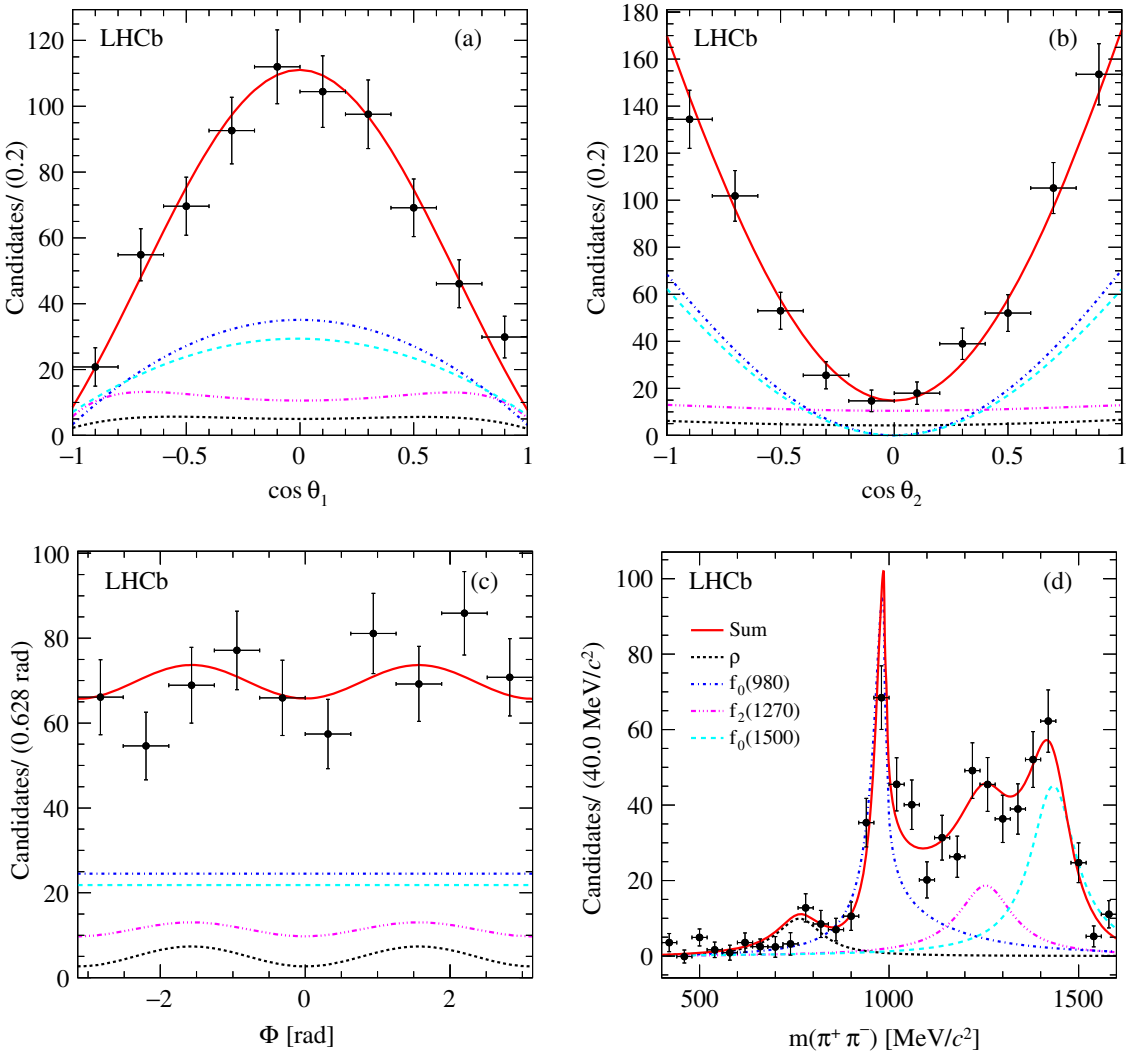

FIG. 7. Projections of (a) $\cos\theta_1$, (b) $\cos\theta_2$, (c) Φ, and (d) $m(\pi^+\pi^-)$ for the preferred fit. The ρ^0 contribution is shown by the dotted (black) line, the $f_0(980)$ by the dot-dashed (blue) line, the $f_2(1270)$ by the double-dot-dashed (magenta) line and the $f_0(1500)$ by the dashed (cyan) line. Note that the expected distributions from each resonance include the effect of the experimental efficiency. The solid (red) line shows the total fit. The points with error bars are the data, where the background has been subtracted using the B_s^0 signal weights from the $K^+K^-\pi^+\pi^-$ invariant mass fit.

TABLE III. The resonance amplitudes and phases from the preferred fit to the $m(\pi^+\pi^-)$ and decay angle distributions of the B_s^0 candidates, including the ρ^0, $f_0(980)$, $f_2(1270)$ and $f_0(1500)$. See text for definitions of the amplitudes and phases.

Amplitude	Fit value	Phase	Fit value (rad)
A_0	0.212 ± 0.035		
$A_\parallel$	0.049 ± 0.031		
$A_\perp$	0.168 ± 0.026	$\delta_\perp$	$+1.90 \pm 0.28$
A_S	0.603 ± 0.036		
A_0^{1270}	0.295 ± 0.058	δ_0^{1270}	-0.62 ± 0.18
$A_\parallel^{1270}$	0.203 ± 0.042	$\delta_\parallel^{1270}$	$+1.26 \pm 0.25$
$A_\perp^{1270}$	0.261 ± 0.037		
A_S^{1500}	0.604 ± 0.031	δ_S^{1500}	$+3.14 \pm 0.30$

summed over the different polarizations and then squared. Interference terms between the resonances are small, but not completely negligible. When calculating the fit fractions and event yields, the interference terms are included in the total yield but not in the individual resonance yields. As a consequence, the sum of the fractions is not 100%. Table IV gives the fit fractions and the corresponding event yields for the resonant contributions to the $B_s^0 \to \phi\pi^+\pi^-$ decay for the fits with and without a ρ^0.

VI. DETERMINATION OF BRANCHING FRACTIONS

The branching fractions are determined using the relationship

TABLE IV. Fit fractions in % and event yields for the resonances contributing to $B_s^0 \to \phi\pi^+\pi^-$. Results are quoted for the preferred model with a ρ^0, and for an alternative model without a ρ^0 which is used to evaluate systematic uncertainties.

Resonance	Fit fractions %		Event yields	
contribution	without ρ^0	with ρ^0	without ρ^0	with ρ^0
ρ^0	–	7.1 ± 1.5	–	50 ± 11
$f_0(980)$	39.5 ± 2.9	35.6 ± 4.3	274 ± 23	247 ± 31
$f_2(1270)$	23.5 ± 2.7	15.1 ± 3.2	163 ± 20	112 ± 23
$f_0(1500)$	26.5 ± 2.2	34.7 ± 3.4	184 ± 17	241 ± 26

$$\frac{\mathcal{B}(B_s^0(B^0) \to \phi\pi^+\pi^-)}{\mathcal{B}(B_s^0 \to \phi\phi)} = \frac{N(\phi\pi^+\pi^-)}{N(\phi\phi)} \times \frac{\varepsilon^{\rm tot}_{\phi\phi}}{\varepsilon^{\rm tot}_{\phi\pi^+\pi^-}} \times \frac{f_s}{f_d} \times \mathcal{B}(\phi \to K^+K^-) \times f_P.$$

The signal yields $N(\phi\pi^+\pi^-)$ for the inclusive modes are taken from the fit to the $K^+K^-\pi^+\pi^-$ mass distribution in Fig. 2, and for the normalization mode $N(\phi\phi)$ is taken from the fit to the $K^+K^-K^+K^-$ mass distribution in Fig. 3. The factor $f_P = (93 \pm 4)\%$ corrects for the difference in the fitted S-wave K^+K^- contributions to the K^+K^- mass distribution around the nominal ϕ mass between the signal and normalization modes. The branching fraction $\mathcal{B}(\phi \to K^+K^-) = (48.9 \pm 0.5)\%$[2] enters twice in the normalization mode. The factor $f_s/f_d = 0.259 \pm 0.015$[31] only applies to the $B^0 \to \phi\pi^+\pi^-$ mode in the above ratio, but also appears in the ratio of $B_s^0 \to \phi\phi$ relative to $B^0 \to \phi K^*$, so it effectively cancels out in the determination of the $B^0 \to \phi\pi^+\pi^-$ branching fraction. For the $B_s^0 \to \phi\pi^+\pi^-$ mode it is included in the determination of $\mathcal{B}(B_s^0 \to \phi\phi)$ [7]. The total selection efficiencies $\varepsilon^{\rm tot}_{\phi\pi^+\pi^-}$ and $\varepsilon^{\rm tot}_{\phi\phi}$ are given in Table V.

TABLE V. Selection efficiencies for the signal and normalization modes in %, as determined from simulated event samples. Here "Initial selection" refers to a loose set of requirements on the four tracks forming the B candidate. The "Offline selection" includes the charm and ϕK^{*0} vetoes, as well as the BDT. Angular acceptance and decay time refer to corrections made for the incorrect modeling of these distributions in the inclusive and $B_s^0 \to \phi f_0(980)$ simulated event samples.

Efficiency	$B_s^0(B^0) \to \phi\pi^+\pi^-$	$B_s^0 \to \phi\rho^0$	$B_s^0 \to \phi f_0(980)$	$B_s^0 \to \phi\phi$
Detector acceptance	17.4	18.1	18.0	17.1
Initial selection	8.43	7.35	8.48	14.6
Trigger	34.9	34.9	34.5	28.6
Offline selection	63.9 (57.1)	62.5	63.2	59.3
Particle identification	87.5	87.5	87.5	93.9
Angular acceptance	95.9 (100)	100	100	100
Decay time	100	100	104.5	100
Total	0.275 (0.256)	0.254	0.303	0.398

For the inclusive modes the branching fractions with $400 < m(\pi^+\pi^-) < 1600$ MeV$/c^2$ are

$$\mathcal{B}(B_s^0 \to \phi\pi^+\pi^-) = [3.48 \pm 0.23] \times 10^{-6},$$

and

$$\mathcal{B}(B^0 \to \phi\pi^+\pi^-) = [1.82 \pm 0.25] \times 10^{-7},$$

where the quoted uncertainties are purely statistical, but include the uncertainties on the yield of the normalization mode, and on the S-wave K^+K^- contributions to the signal and normalization modes. For the exclusive B_s^0 modes the signal yields are taken from the final column in Table IV. The branching fractions are

$$\mathcal{B}(B_s^0 \to \phi f_0(980)) = [1.12 \pm 0.16] \times 10^{-6},$$
$$\mathcal{B}(B_s^0 \to \phi f_2(1270)) = [0.61 \pm 0.13] \times 10^{-6},$$

and

$$\mathcal{B}(B_s^0 \to \phi\rho^0) = [2.7 \pm 0.6] \times 10^{-7}.$$

The remaining 1.5×10^{-6} of the inclusive B_s^0 branching fraction is mostly accounted for by an S-wave contribution in the region 1350–1600 MeV$/c^2$ as discussed in the previous section.

TABLE VI. Systematic uncertainties in % on the branching fractions of B_s^0 and B^0 decays. All the uncertainties are taken on the ratio of the signal to the normalization mode. Uncertainties marked by a dash are either negligible or exactly zero. The asymmetric uncertainties on $\phi f_0(980)$ and $\phi f_2(1270)$ come from the differences in yields between the fits with and without the ρ^0 contribution.

Systematic	$B_s^0 \to \phi\rho^0$	$B_s^0 \to \phi f_0(980)$	$B_s^0 \to \phi f_2(1270)$	$B_s^0(B^0) \to \phi\pi^+\pi^-$
Trigger	0.5	0.5	0.5	0.5
Hadronic interactions	0.5	0.5	0.5	0.5
Offline selection	2.3	2.3	2.3	2.3
Particle identification	0.3	0.3	0.3	0.3
Angular acceptance	3.8	–	3.8	3.8 (10.7)
Decay time acceptance	1.1	1.1	1.1	1.1 (–)
$m(K^+K^-\pi^+\pi^-)$ fit	1.2	1.2	1.2	1.2 (19.5)
Amplitude analysis	2.5	$+4.7/-0.4$	$+17.6/-2.7$	–
S-wave K^+K^-	6.0	6.0	6.0	–
Total	7.0	$+8.2/-6.7$	$+19.2/-8.1$	4.8 (22.4)

VII. SYSTEMATIC UNCERTAINTIES

Many systematic effects cancel in the ratio of efficiencies between the signal and normalization modes. The remaining systematic uncertainties in the determination of the branching fractions come from replacing the $\pi^+\pi^-$ pair with a second ϕ meson decaying to two kaons. The systematic uncertainties are summarized in Table VI.

The trigger selection has a different performance for the $B_s^0 \to \phi\pi^+\pi^-$ signal and for the $B_s^0 \to \phi\phi$ normalization mode due to the different kinematics of the final state hadrons. The simulation of the trigger does not reproduce this difference accurately for hadronic decays, and a $D^0 \to K^-\pi^+$ control sample, collected with a minimum bias trigger, is used to evaluate corrections to the trigger efficiencies between the simulation and the data. These are applied as per-event reweightings of the simulation as a function of track p_T, particle type K or π, and magnetic field orientation. For both the signal and normalization modes there are large corrections of ≈30%, but they almost completely cancel in the ratio, leaving a systematic uncertainty of 0.5% from this source.

Another aspect of the detector efficiency that is not accurately modeled by the simulation is hadronic interactions in the detector. A sample of simulated $B^0 \to J/\psi K^{*0}$ events is used to determine the fraction of kaons and pions that interact within the detector as a function of their momentum. On average this varies from 11% for K^+ to 15% for π^-. These numbers are then scaled up to account for additional material in the detector compared to the simulation. The effect partly cancels in the ratio of the signal and normalization modes leaving a 0.5% systematic uncertainty from this source.

The offline selection efficiency has an uncertainty coming from the performance of the multivariate BDT. This has been studied by varying the selection on the $B_s^0 \to \phi\phi$ normalization mode, and extracting the shapes of the input variables from data using the *sPlot* technique. The distributions agree quite well between simulation and data, but there are small differences. When these are propagated to the signal modes they lead to a reduction in the BDT efficiency. Again the effect partially cancels in the ratio leaving a systematic uncertainty of 2.3%.

The offline selection also has an uncertainty coming from the different particle identification criteria used for the $\pi^+\pi^-$ in the signal and the K^+K^- from the second ϕ in the normalization mode. Corrections between simulation and data are studied using calibration samples, with kaons and pions binned in p_T, η and number of tracks in the event. There is an uncertainty of 0.1% from the size of the calibration samples. Using different binning schemes for the corrections leads to a slightly higher estimate for the systematic uncertainty of 0.3%.

For the angular acceptance there is an uncertainty in the $m(\pi^+\pi^-)$ and angular distributions for the inclusive decays, and in the polarizations of the ρ^0 and $f_2(1270)$. A three-dimensional binning in $[\cos\theta_1, \cos\theta_2, m(\pi^+\pi^-)]$ is used to reweight the simulation to match the data distributions for these modes. The accuracy of this procedure is limited by the number of bins and hence by the data statistics. By varying the binning scheme, systematic uncertainties of 3.8% (10.7%) are determined for B_s^0 (B^0) from this reweighting procedure. The larger B^0 uncertainty reflects the smaller signal yield. The angular distribution of the $B_s^0 \to \phi\phi$ normalization mode is modeled according to the published LHCb measurements [4], which introduces a negligible uncertainty.

The decay time acceptance of the detector falls off rapidly at short decay times due to the requirement that the tracks are consistent with coming from a secondary vertex. For B_s^0 decays the decay time distribution is modeled by the flavor-specific lifetime, but it should be modeled by a combination of the heavy and light mass eigenstates, depending on the decay mode. A systematic uncertainty of 1.1% is found when replacing the flavor-specific lifetime by the lifetime of the heavy eigenstate and determining the change in the decay time acceptance. There is no effect on B^0 decays or on the normalization mode where the lifetime is modeled according to the published measurements.

The $K^+K^-\pi^+\pi^-$ and $K^+K^-K^+K^-$ invariant mass fits are repeated using a single Gaussian and using a power-law function to model the tails of the signal shapes. For the $m(K^+K^-\pi^+\pi^-)$ fit contributions from partially reconstructed backgrounds are added, including $B_s^0 \to \phi\phi(\pi^+\pi^-\pi^0)$ and $B_s^0 \to \phi\eta'(\pi^+\pi^-\gamma)$. These changes lead to uncertainties on the B_s^0 (B^0) yields of 1.2% (19.5%). The large uncertainty on the B^0 yield comes both from the change in the signal shape and from the addition of partially reconstructed B_s^0 backgrounds. This systematic uncertainty reduces the significance of the B^0 signal from 7.7σ to 4.5σ.

The results of the amplitude analysis for the exclusive B_s^0 decays depend on the set of input resonances that are used. The effect of including the ρ^0 is treated as a systematic uncertainty on the $f_0(980)$ and $f_2(1270)$ yields (see Table IV). The effect of adding either an $f_0(500)$ or a $\rho(1450)$ is treated as a systematic uncertainty on all the exclusive modes.

The difference between the S-wave K^+K^- components in the signal and normalization modes is measured to be $(7.1 \pm 4.0)\%$ from fits to the K^+K^- mass distributions. The uncertainty on this is treated as part of the statistical error. However, the S-wave component of the signal sample was not included in the amplitude analysis where it would give a flat distribution in $\cos\theta_2$. A study of the dependence of the S-wave K^+K^- component as a function of $m(\pi^+\pi^-)$ does not indicate a significant variation, and the statistical uncertainty of 6% from this study is taken as a systematic uncertainty on the yields of the exclusive modes extracted from the amplitude analysis.

VIII. SUMMARY AND CONCLUSIONS

This paper reports the first observation of the inclusive decay $B_s^0 \to \phi\pi^+\pi^-$. The branching fraction in the mass range $400 < m(\pi^+\pi^-) < 1600\ \mathrm{MeV}/c^2$ is measured to be

$$\mathcal{B}(B_s^0 \to \phi\pi^+\pi^-) = [3.48 \pm 0.23 \pm 0.17 \pm 0.35] \times 10^{-6},$$

where the first uncertainty is statistical, the second is systematic, and the third is due to the normalization mode $B_s^0 \to \phi\phi$.

Evidence is also seen for the inclusive decay $B^0 \to \phi\pi^+\pi^-$ with a statistical significance of 7.7σ, which is reduced to 4.5σ after taking into account the systematic uncertainties on the signal yield. The branching fraction in the mass range $400 < m(\pi^+\pi^-) < 1600\ \mathrm{MeV}/c^2$ is

$$\mathcal{B}(B^0 \to \phi\pi^+\pi^-) = [1.82 \pm 0.25 \pm 0.41 \pm 0.14] \times 10^{-7}.$$

An amplitude analysis is used to separate out exclusive contributions to the B_s^0 decays. The decay $B_s^0 \to \phi f_0(980)$ is observed with a significance of 8σ, and the product branching fraction is

$$\mathcal{B}(B_s^0 \to \phi f_0(980), f_0(980) \to \pi^+\pi^-) = [1.12 \pm 0.16^{+0.09}_{-0.08} \pm 0.11] \times 10^{-6}.$$

The decay $B_s^0 \to \phi f_2(1270)$ is observed with a significance of 5σ, and the product branching fraction is

$$\mathcal{B}(B_s^0 \to \phi f_2(1270), f_2(1270) \to \pi^+\pi^-) = [0.61 \pm 0.13^{+0.12}_{-0.05} \pm 0.06] \times 10^{-6}.$$

There is also a contribution from higher mass S-wave $\pi^+\pi^-$ states in the region 1350–1600 MeV/c^2, which could be ascribed to a linear superposition of the $f_0(1370)$ and the $f_0(1500)$. There is 4σ evidence for the decay $B_s^0 \to \phi\rho^0$ with a branching fraction of

$$\mathcal{B}(B_s^0 \to \phi\rho^0) = [2.7 \pm 0.7 \pm 0.2 \pm 0.2] \times 10^{-7}.$$

This is lower than the Standard Model prediction of $[4.4^{+2.2}_{-0.7}] \times 10^{-7}$, but still consistent with it, and provides a constraint on possible contributions from new physics in this decay.

With more data coming from the LHC it will be possible to further investigate the exclusive decays, perform an amplitude analysis of the B^0 decays, and eventually make measurements of time-dependent CP violation that are complementary to the measurements already made in the $B_s^0 \to \phi\phi$ decay.

ACKNOWLEDGMENTS

We express our gratitude to our colleagues in the CERN accelerator departments for the excellent performance of the LHC. We thank the technical and administrative staff at the LHCb institutes. We acknowledge support from CERN and from the national agencies: CAPES, CNPq, FAPERJ and FINEP (Brazil); NSFC (China); CNRS/IN2P3 (France); BMBF, DFG and MPG (Germany); INFN (Italy); FOM and NWO (The Netherlands); MNiSW and NCN (Poland); MEN/IFA (Romania); MinES and FASO (Russia); MinECo (Spain); SNSF and SER (Switzerland); NASU (Ukraine); STFC (United Kingdom); NSF (USA). We acknowledge the computing resources that are provided by CERN, IN2P3 (France), KIT and DESY (Germany), INFN (Italy), SURF (The Netherlands), PIC (Spain), GridPP (United Kingdom), RRCKI and Yandex LLC (Russia), CSCS (Switzerland), IFIN-HH (Romania), CBPF (Brazil), PL-GRID (Poland) and OSC (USA). We are indebted to the communities behind the multiple open source software packages on which we depend. Individual groups or members have received support from AvH Foundation (Germany), EPLANET, Marie Skłodowska-Curie Actions and ERC (European Union), Conseil Général de Haute-Savoie, Labex ENIGMASS and OCEVU, Région Auvergne (France), RFBR and Yandex LLC (Russia), GVA, XuntaGal and GENCAT (Spain), Herchel Smith Fund, The Royal Society, Royal Commission for the Exhibition of 1851 and the Leverhulme Trust (United Kingdom).

[1] M. Raidal, *CP* Asymmetry in $B \to \phi K_S$ Decays in Left-Right Models and Its Implications for B_s Decays, Phys. Rev. Lett. **89**, 231803 (2002).

[2] K. A. Olive *et al.* (Particle Data Group), Review of particle physics, Chin. Phys. C **38**, 090001 (2014).

[3] R. Aaij *et al.* (LHCb Collaboration), First Measurement of the *CP*-Violating Phase in $B_s^0 \to \phi\phi$ Decays, Phys. Rev. Lett. **110**, 241802 (2013).

[4] R. Aaij *et al.* (LHCb Collaboration), Measurement of *CP* violation in $B_s^0 \to \phi\phi$ decays, Phys. Rev. D **90**, 052011 (2014).

[5] L. Hofer, D. Scherer, and L. Vernazza, $B_s \to \phi\rho^0$ and $B_s \to \phi\pi^0$ as a handle on isospin-violating new physics, J. High Energy Phys. 02 (2011) 080.

[6] B. Aubert *et al.* (*BABAR* Collaboration), Searches for B Meson Decays to $\phi\phi, \phi\rho, \phi f_0(980)$, and $f_0(980)f_0(980)$ Final States, Phys. Rev. Lett. **101**, 201801 (2008).

[7] R. Aaij *et al.* (LHCb Collaboration), Measurement of the $B_s^0 \to \phi\phi$ branching fraction and search for the decay $B^0 \to \phi\phi$, J. High Energy Phys. 10 (2015) 053.
[8] B. Aubert *et al.* (*BABAR* Collaboration), Time-dependent and time-integrated angular analysis of $B^0 \to \phi K_S^0 \pi^0$ and $B^0 \to \phi K^+ \pi^-$, Phys. Rev. D **78**, 092008 (2008).
[9] M. Prim *et al.* (Belle Collaboration), Angular analysis of $B^0 \to \phi K^*$ decays and search for *CP* violation at Belle, Phys. Rev. D **88**, 072004 (2013).
[10] A. A. Alves Jr. *et al.* (LHCb Collaboration), The LHCb Detector at the LHC, J. Instrum. **3**, S08005 (2008).
[11] R. Aaij *et al.* (LHCb Collaboration), LHCb detector performance, Int. J. Mod. Phys. A **30**, 1530022 (2015).
[12] R. Aaij *et al.*, The LHCb trigger and its performance in 2011, J. Instrum. **8**, P04022 (2013).
[13] V. V. Gligorov and M. Williams, Efficient, reliable and fast high-level triggering using a bonsai boosted decision tree, J. Instrum. **8**, P02013 (2013).
[14] T. Sjöstrand, S. Mrenna, and P. Skands, PYTHIA 6.4 physics and manual, J. High Energy Phys. 05 (2006) 026.
[15] I. Belyaev *et al.*, Handling of the generation of primary events in Gauss, the LHCb simulation framework, J. Phys. Conf. Ser. **331**, 032047 (2011).
[16] D. J. Lange, The EvtGen particle decay simulation package, Nucl. Instrum. Methods Phys. Res., Sect. A **462**, 152 (2001).
[17] P. Golonka and Z. Was, PHOTOS Monte Carlo: A precision tool for QED corrections in Z and W decays, Eur. Phys. J. C **45**, 97 (2006).
[18] J. Allison *et al.* (Geant4 Collaboration), Geant4 developments and applications, IEEE Trans. Nucl. Sci. **53**, 270 (2006); S. Agostinelli *et al.* (Geant4 Collaboration), Geant4: A simulation toolkit, Nucl. Instrum. Methods Phys. Res., Sect. A **506**, 250 (2003).
[19] M. Clemencic *et al.*, The LHCb simulation application, Gauss: Design, evolution and experience, J. Phys. Conf. Ser. **331**, 032023 (2011).
[20] L. Breiman, J. H. Friedman, R. A. Olshen, and C. J. Stone, *Classification and Regression Trees* (Wadsworth International Group, Belmont, CA, 1984).
[21] Y. Freund and R. E. Schapire, A decision-theoretic generalization of on-line learning and an application to boosting, J. Comput. Syst. Sci. **55**, 119 (1997).
[22] G. Punzi, in *Statistical Problems in Particle Physics, Astrophysics, and Cosmology*, edited by L. Lyons, R. Mount, and R. Reitmeyer, arXiv:physics/0308063.
[23] M. Pivk and F. R. Le Diberder, sPlot: A statistical tool to unfold data distributions, Nucl. Instrum. Methods Phys. Res., Sect. A **555**, 356 (2005).
[24] D. V. Bugg, Review of scalar mesons, AIP Conf. Proc. **1030**, 3 (2008).
[25] D. V. Bugg, The mass of the σ pole, J. Phys. G **34**, 151 (2007).
[26] S. M. Flatté, On the nature of 0+ mesons, Phys. Lett. B **63**, 228 (1976).
[27] R. Aaij *et al.* (LHCb Collaboration), Analysis of the resonant components in $\bar{B}_s^0 \to J/\psi\pi^+\pi^-$, Phys. Rev. D **86**, 052006 (2012).
[28] J. E. Augustin *et al.* (DM2 Collaboration), Radiative decay of J/ψ into $\gamma\pi^+\pi^-$, Z. Phys. C **36**, 369 (1987).
[29] R. Aaij *et al.* (LHCb Collaboration), Measurement of resonant and *CP* components in $\bar{B}_s^0 \to J/\psi\pi^+\pi^-$ decays, Phys. Rev. D **89**, 092006 (2014).
[30] F. E. Close and A. Kirk, Interpretation of scalar and axial mesons in LHCb from a historical perspective, Phys. Rev. D **91**, 114015 (2015).
[31] R. Aaij *et al.* (LHCb Collaboration), Measurement of the fragmentation fraction ratio f_s/f_d and its dependence on B meson kinematics, J. High Energy Phys. 04 (2013) 001.

R. Aaij,[40] B. Adeva,[39] M. Adinolfi,[48] Z. Ajaltouni,[5] S. Akar,[6] J. Albrecht,[10] F. Alessio,[40] M. Alexander,[53] S. Ali,[43] G. Alkhazov,[31] P. Alvarez Cartelle,[55] A. A. Alves Jr.,[59] S. Amato,[2] S. Amerio,[23] Y. Amhis,[7] L. An,[41] L. Anderlini,[18] G. Andreassi,[41] M. Andreotti,[17,a] J. E. Andrews,[60] R. B. Appleby,[56] F. Archilli,[43] P. d'Argent,[12] J. Arnau Romeu,[6] A. Artamonov,[37] M. Artuso,[61] E. Aslanides,[6] G. Auriemma,[26] M. Baalouch,[5] I. Babuschkin,[56] S. Bachmann,[12] J. J. Back,[50] A. Badalov,[38] C. Baesso,[62] S. Baker,[55] W. Baldini,[17] R. J. Barlow,[56] C. Barschel,[40] S. Barsuk,[7] W. Barter,[40] M. Baszczyk,[27] V. Batozskaya,[29] B. Batsukh,[61] V. Battista,[41] A. Bay,[41] L. Beaucourt,[4] J. Beddow,[53] F. Bedeschi,[24] I. Bediaga,[1] L. J. Bel,[43] V. Bellee,[41] N. Belloli,[21,b] K. Belous,[37] I. Belyaev,[32] E. Ben-Haim,[8] G. Bencivenni,[19] S. Benson,[43] J. Benton,[48] A. Berezhnoy,[33] R. Bernet,[42] A. Bertolin,[23] F. Betti,[15] M.-O. Bettler,[40] M. van Beuzekom,[43] Ia. Bezshyiko,[42] S. Bifani,[47] P. Billoir,[8] T. Bird,[56] A. Birnkraut,[10] A. Bitadze,[56] A. Bizzeti,[18,c] T. Blake,[50] F. Blanc,[41] J. Blouw,[11] S. Blusk,[61] V. Bocci,[26] T. Boettcher,[58] A. Bondar,[36,d] N. Bondar,[31,40] W. Bonivento,[16] A. Borgheresi,[21,b] S. Borghi,[56] M. Borisyak,[35] M. Borsato,[39] F. Bossu,[7] M. Boubdir,[9] T. J. V. Bowcock,[54] E. Bowen,[42] C. Bozzi,[17,40] S. Braun,[12] M. Britsch,[12] T. Britton,[61] J. Brodzicka,[56] E. Buchanan,[48] C. Burr,[56] A. Bursche,[2] J. Buytaert,[40] S. Cadeddu,[16] R. Calabrese,[17,a] M. Calvi,[21,b] M. Calvo Gomez,[38,e] A. Camboni,[38] P. Campana,[19] D. Campora Perez,[40] D. H. Campora Perez,[40] L. Capriotti,[56] A. Carbone,[15,f] G. Carboni,[25,g] R. Cardinale,[20,h] A. Cardini,[16] P. Carniti,[21,b] L. Carson,[52] K. Carvalho Akiba,[2] G. Casse,[54] L. Cassina,[21,b] L. Castillo Garcia,[41] M. Cattaneo,[40] Ch. Cauet,[10] G. Cavallero,[20] R. Cenci,[24,i] M. Charles,[8] Ph. Charpentier,[40] G. Chatzikonstantinidis,[47] M. Chefdeville,[4] S. Chen,[56] S.-F. Cheung,[57] V. Chobanova,[39] M. Chrzaszcz,[42,27] X. Cid Vidal,[39] G. Ciezarek,[43] P. E. L. Clarke,[52] M. Clemencic,[40] H. V. Cliff,[49] J. Closier,[40] V. Coco,[59] J. Cogan,[6] E. Cogneras,[5]

V. Cogoni,[16,40,j] L. Cojocariu,[30] G. Collazuol,[23,k] P. Collins,[40] A. Comerma-Montells,[12] A. Contu,[40] A. Cook,[48] S. Coquereau,[38] G. Corti,[40] M. Corvo,[17,a] C. M. Costa Sobral,[50] B. Couturier,[40] G. A. Cowan,[52] D. C. Craik,[52] A. Crocombe,[50] M. Cruz Torres,[62] S. Cunliffe,[55] R. Currie,[55] C. D'Ambrosio,[40] E. Dall'Occo,[43] J. Dalseno,[48] P. N. Y. David,[43] A. Davis,[59] O. De Aguiar Francisco,[2] K. De Bruyn,[6] S. De Capua,[56] M. De Cian,[12] J. M. De Miranda,[1] L. De Paula,[2] M. De Serio,[14,l] P. De Simone,[19] C.-T. Dean,[53] D. Decamp,[4] M. Deckenhoff,[10] L. Del Buono,[8] M. Demmer,[10] D. Derkach,[35] O. Deschamps,[5] F. Dettori,[40] B. Dey,[22] A. Di Canto,[40] H. Dijkstra,[40] F. Dordei,[40] M. Dorigo,[41] A. Dosil Suárez,[39] A. Dovbnya,[45] K. Dreimanis,[54] L. Dufour,[43] G. Dujany,[56] K. Dungs,[40] P. Durante,[40] R. Dzhelyadin,[37] A. Dziurda,[40] A. Dzyuba,[31] N. Déléage,[4] S. Easo,[51] M. Ebert,[52] U. Egede,[55] V. Egorychev,[32] S. Eidelman,[36,d] S. Eisenhardt,[52] U. Eitschberger,[10] R. Ekelhof,[10] L. Eklund,[53] Ch. Elsasser,[42] S. Ely,[61] S. Esen,[12] H. M. Evans,[49] T. Evans,[57] A. Falabella,[15] N. Farley,[47] S. Farry,[54] R. Fay,[54] D. Fazzini,[21,b] D. Ferguson,[52] V. Fernandez Albor,[39] A. Fernandez Prieto,[39] F. Ferrari,[15,40] F. Ferreira Rodrigues,[1] M. Ferro-Luzzi,[40] S. Filippov,[34] R. A. Fini,[14] M. Fiore,[17,a] M. Fiorini,[17,a] M. Firlej,[28] C. Fitzpatrick,[41] T. Fiutowski,[28] F. Fleuret,[7,m] K. Fohl,[40] M. Fontana,[16] F. Fontanelli,[20,h] D. C. Forshaw,[61] R. Forty,[40] V. Franco Lima,[54] M. Frank,[40] C. Frei,[40] J. Fu,[22,n] E. Furfaro,[25,g] C. Färber,[40] A. Gallas Torreira,[39] D. Galli,[15,f] S. Gallorini,[23] S. Gambetta,[52] M. Gandelman,[2] P. Gandini,[57] Y. Gao,[3] L. M. Garcia Martin,[68] J. García Pardiñas,[39] J. Garra Tico,[49] L. Garrido,[38] P. J. Garsed,[49] D. Gascon,[38] C. Gaspar,[40] L. Gavardi,[10] G. Gazzoni,[5] D. Gerick,[12] E. Gersabeck,[12] M. Gersabeck,[56] T. Gershon,[50] Ph. Ghez,[4] S. Gianì,[41] V. Gibson,[49] O. G. Girard,[41] L. Giubega,[30] K. Gizdov,[52] V. V. Gligorov,[8] D. Golubkov,[32] A. Golutvin,[55,40] A. Gomes,[1,o] I. V. Gorelov,[33] C. Gotti,[21,b] M. Grabalosa Gándara,[5] R. Graciani Diaz,[38] L. A. Granado Cardoso,[40] E. Graugés,[38] E. Graverini,[42] G. Graziani,[18] A. Grecu,[30] P. Griffith,[47] L. Grillo,[21,b] B. R. Gruberg Cazon,[57] O. Grünberg,[66] E. Gushchin,[34] Yu. Guz,[37] T. Gys,[40] C. Göbel,[62] T. Hadavizadeh,[57] C. Hadjivasiliou,[5] G. Haefeli,[41] C. Haen,[40] S. C. Haines,[49] S. Hall,[55] B. Hamilton,[60] X. Han,[12] S. Hansmann-Menzemer,[12] N. Harnew,[57] S. T. Harnew,[48] J. Harrison,[56] M. Hatch,[40] J. He,[63] T. Head,[41] A. Heister,[9] K. Hennessy,[54] P. Henrard,[5] L. Henry,[8] J. A. Hernando Morata,[39] E. van Herwijnen,[40] M. Heß,[66] A. Hicheur,[2] D. Hill,[57] C. Hombach,[56] H. Hopchev,[41] W. Hulsbergen,[43] T. Humair,[55] M. Hushchyn,[35] N. Hussain,[57] D. Hutchcroft,[54] M. Idzik,[28] P. Ilten,[58] R. Jacobsson,[40] A. Jaeger,[12] J. Jalocha,[57] E. Jans,[43] A. Jawahery,[60] F. Jiang,[3] M. John,[57] D. Johnson,[40] C. R. Jones,[49] C. Joram,[40] B. Jost,[40] N. Jurik,[61] S. Kandybei,[45] W. Kanso,[6] M. Karacson,[40] J. M. Kariuki,[48] S. Karodia,[53] M. Kecke,[12] M. Kelsey,[61] I. R. Kenyon,[47] M. Kenzie,[40] T. Ketel,[44] E. Khairullin,[35] B. Khanji,[21,40,b] C. Khurewathanakul,[41] T. Kirn,[9] S. Klaver,[56] K. Klimaszewski,[29] S. Koliiev,[46] M. Kolpin,[12] I. Komarov,[41] R. F. Koopman,[44] P. Koppenburg,[43] A. Kozachuk,[33] M. Kozeiha,[5] L. Kravchuk,[34] K. Kreplin,[12] M. Kreps,[50] P. Krokovny,[36,d] F. Kruse,[10] W. Krzemien,[29] W. Kucewicz,[27,p] M. Kucharczyk,[27] V. Kudryavtsev,[36,d] A. K. Kuonen,[41] K. Kurek,[29] T. Kvaratskheliya,[32,40] D. Lacarrere,[40] G. Lafferty,[56,40] A. Lai,[16] D. Lambert,[52] G. Lanfranchi,[19] C. Langenbruch,[9] T. Latham,[50] C. Lazzeroni,[47] R. Le Gac,[6] J. van Leerdam,[43] J.-P. Lees,[4] A. Leflat,[33,40] J. Lefrançois,[7] R. Lefèvre,[5] F. Lemaitre,[40] E. Lemos Cid,[39] O. Leroy,[6] T. Lesiak,[27] B. Leverington,[12] Y. Li,[7] T. Likhomanenko,[35,67] R. Lindner,[40] C. Linn,[40] F. Lionetto,[42] B. Liu,[16] X. Liu,[3] D. Loh,[50] I. Longstaff,[53] J. H. Lopes,[2] D. Lucchesi,[23,k] M. Lucio Martinez,[39] H. Luo,[52] A. Lupato,[23] E. Luppi,[17,a] O. Lupton,[57] A. Lusiani,[24] X. Lyu,[63] F. Machefert,[7] F. Maciuc,[30] O. Maev,[31] K. Maguire,[56] S. Malde,[57] A. Malinin,[67] T. Maltsev,[36] G. Manca,[7] G. Mancinelli,[6] P. Manning,[61] J. Maratas,[5,q] J. F. Marchand,[4] U. Marconi,[15] C. Marin Benito,[38] P. Marino,[24,i] J. Marks,[12] G. Martellotti,[26] M. Martin,[6] M. Martinelli,[41] D. Martinez Santos,[39] F. Martinez Vidal,[68] D. Martins Tostes,[2] L. M. Massacrier,[7] A. Massafferri,[1] R. Matev,[40] A. Mathad,[50] Z. Mathe,[40] C. Matteuzzi,[21] A. Mauri,[42] B. Maurin,[41] A. Mazurov,[47] M. McCann,[55] J. McCarthy,[47] A. McNab,[56] R. McNulty,[13] B. Meadows,[59] F. Meier,[10] M. Meissner,[12] D. Melnychuk,[29] M. Merk,[43] A. Merli,[22,n] E. Michielin,[23] D. A. Milanes,[65] M.-N. Minard,[4] D. S. Mitzel,[12] A. Mogini,[8] J. Molina Rodriguez,[62] I. A. Monroy,[65] S. Monteil,[5] M. Morandin,[23] P. Morawski,[28] A. Mordà,[6] M. J. Morello,[24,i] J. Moron,[28] A. B. Morris,[52] R. Mountain,[61] F. Muheim,[52] M. Mulder,[43] M. Mussini,[15] D. Müller,[56] J. Müller,[10] K. Müller,[42] V. Müller,[10] P. Naik,[48] T. Nakada,[41] R. Nandakumar,[51] A. Nandi,[57] I. Nasteva,[2] M. Needham,[52] N. Neri,[22] S. Neubert,[12] N. Neufeld,[40] M. Neuner,[12] A. D. Nguyen,[41] C. Nguyen-Mau,[41,r] S. Nieswand,[9] R. Niet,[10] N. Nikitin,[33] T. Nikodem,[12] A. Novoselov,[37] D. P. O'Hanlon,[50] A. Oblakowska-Mucha,[28] V. Obraztsov,[37] S. Ogilvy,[19] R. Oldeman,[49] C. J. G. Onderwater,[69] J. M. Otalora Goicochea,[2] A. Otto,[40] P. Owen,[42] A. Oyanguren,[68] P. R. Pais,[41] A. Palano,[14,l] F. Palombo,[22,n] M. Palutan,[19] J. Panman,[40] A. Papanestis,[51] M. Pappagallo,[14,l] L. L. Pappalardo,[17,a] W. Parker,[60] C. Parkes,[56] G. Passaleva,[18] A. Pastore,[14,l] G. D. Patel,[54] M. Patel,[55] C. Patrignani,[15,f] A. Pearce,[56,51] A. Pellegrino,[43] G. Penso,[26] M. Pepe Altarelli,[40] S. Perazzini,[40] P. Perret,[5] L. Pescatore,[47] K. Petridis,[48] A. Petrolini,[20,h] A. Petrov,[67] M. Petruzzo,[22,n] E. Picatoste Olloqui,[38] B. Pietrzyk,[4] M. Pikies,[27] D. Pinci,[26] A. Pistone,[20] A. Piucci,[12] S. Playfer,[52] M. Plo Casasus,[39]

T. Poikela,[40] F. Polci,[8] A. Poluektov,[50,36] I. Polyakov,[61] E. Polycarpo,[2] G. J. Pomery,[48] A. Popov,[37] D. Popov,[11,40] B. Popovici,[30] S. Poslavskii,[37] C. Potterat,[2] E. Price,[48] J. D. Price,[54] J. Prisciandaro,[39] A. Pritchard,[54] C. Prouve,[48] V. Pugatch,[46] A. Puig Navarro,[41] G. Punzi,[24,s] W. Qian,[57] R. Quagliani,[7,48] B. Rachwal,[27] J. H. Rademacker,[48] M. Rama,[24] M. Ramos Pernas,[39] M. S. Rangel,[2] I. Raniuk,[45] G. Raven,[44] F. Redi,[55] S. Reichert,[10] A. C. dos Reis,[1] C. Remon Alepuz,[68] V. Renaudin,[7] S. Ricciardi,[51] S. Richards,[48] M. Rihl,[40] K. Rinnert,[54,40] V. Rives Molina,[38] P. Robbe,[7,40] A. B. Rodrigues,[1] E. Rodrigues,[59] J. A. Rodriguez Lopez,[65] P. Rodriguez Perez,[56] A. Rogozhnikov,[35] S. Roiser,[40] V. Romanovskiy,[37] A. Romero Vidal,[39] J. W. Ronayne,[13] M. Rotondo,[19] M. S. Rudolph,[61] T. Ruf,[40] P. Ruiz Valls,[68] J. J. Saborido Silva,[39] E. Sadykhov,[32] N. Sagidova,[31] B. Saitta,[16,j] V. Salustino Guimaraes,[2] C. Sanchez Mayordomo,[68] B. Sanmartin Sedes,[39] R. Santacesaria,[26] C. Santamarina Rios,[39] M. Santimaria,[19] E. Santovetti,[25,g] A. Sarti,[19,t] C. Satriano,[26,u] A. Satta,[25] D. M. Saunders,[48] D. Savrina,[32,33] S. Schael,[9] M. Schellenberg,[10] M. Schiller,[40] H. Schindler,[40] M. Schlupp,[10] M. Schmelling,[11] T. Schmelzer,[10] B. Schmidt,[40] O. Schneider,[41] A. Schopper,[40] K. Schubert,[10] M. Schubiger,[41] M.-H. Schune,[7] R. Schwemmer,[40] B. Sciascia,[19] A. Sciubba,[26,t] A. Semennikov,[32] A. Sergi,[47] N. Serra,[42] J. Serrano,[6] L. Sestini,[23] P. Seyfert,[21] M. Shapkin,[37] I. Shapoval,[45] Y. Shcheglov,[31] T. Shears,[54] L. Shekhtman,[36,d] V. Shevchenko,[67] A. Shires,[10] B. G. Siddi,[17] R. Silva Coutinho,[42] L. Silva de Oliveira,[2] G. Simi,[23,k] S. Simone,[14,l] M. Sirendi,[49] N. Skidmore,[48] T. Skwarnicki,[61] E. Smith,[55] I. T. Smith,[52] J. Smith,[49] M. Smith,[55] H. Snoek,[43] M. D. Sokoloff,[59] F. J. P. Soler,[53] D. Souza,[48] B. Souza De Paula,[2] B. Spaan,[10] P. Spradlin,[53] S. Sridharan,[40] F. Stagni,[40] M. Stahl,[12] S. Stahl,[40] P. Stefko,[41] S. Stefkova,[55] O. Steinkamp,[42] S. Stemmle,[12] O. Stenyakin,[37] S. Stevenson,[57] S. Stoica,[30] S. Stone,[61] B. Storaci,[42] S. Stracka,[24,s] M. Straticiuc,[30] U. Straumann,[42] L. Sun,[59] W. Sutcliffe,[55] K. Swientek,[28] V. Syropoulos,[44] M. Szczekowski,[29] T. Szumlak,[28] S. T'Jampens,[4] A. Tayduganov,[6] T. Tekampe,[10] M. Teklishyn,[7] G. Tellarini,[17,a] F. Teubert,[40] C. Thomas,[57] E. Thomas,[40] J. van Tilburg,[43] M. J. Tilley,[55] V. Tisserand,[4] M. Tobin,[41] S. Tolk,[49] L. Tomassetti,[17,a] D. Tonelli,[40] S. Topp-Joergensen,[57] F. Toriello,[61] E. Tournefier,[4] S. Tourneur,[41] K. Trabelsi,[41] M. Traill,[53] M. T. Tran,[41] M. Tresch,[42] A. Trisovic,[40] A. Tsaregorodtsev,[6] P. Tsopelas,[43] A. Tully,[49] N. Tuning,[43] A. Ukleja,[29] A. Ustyuzhanin,[35,67] U. Uwer,[12] C. Vacca,[16,40,j] V. Vagnoni,[15,40] A. Valassi,[40] S. Valat,[40] G. Valenti,[15] A. Vallier,[7] R. Vazquez Gomez,[19] P. Vazquez Regueiro,[39] S. Vecchi,[17] M. van Veghel,[43] J. J. Velthuis,[48] M. Veltri,[18,v] G. Veneziano,[41] A. Venkateswaran,[61] M. Vernet,[5] M. Vesterinen,[12] B. Viaud,[7] D. Vieira,[1] M. Vieites Diaz,[39] X. Vilasis-Cardona,[38,e] V. Volkov,[33] A. Vollhardt,[42] B. Voneki,[40] A. Vorobyev,[31] V. Vorobyev,[36,d] C. Voß,[66] J. A. de Vries,[43] C. Vázquez Sierra,[39] R. Waldi,[66] C. Wallace,[50] R. Wallace,[13] J. Walsh,[24] J. Wang,[61] D. R. Ward,[49] H. M. Wark,[54] N. K. Watson,[47] D. Websdale,[55] A. Weiden,[42] M. Whitehead,[40] J. Wicht,[50] G. Wilkinson,[57,40] M. Wilkinson,[61] M. Williams,[40] M. P. Williams,[47] M. Williams,[58] T. Williams,[47] F. F. Wilson,[51] J. Wimberley,[60] J. Wishahi,[10] W. Wislicki,[29] M. Witek,[27] G. Wormser,[7] S. A. Wotton,[49] K. Wraight,[53] S. Wright,[49] K. Wyllie,[40] Y. Xie,[64] Z. Xing,[61] Z. Xu,[41] Z. Yang,[3] H. Yin,[64] J. Yu,[64] X. Yuan,[36,d] O. Yushchenko,[37] M. Zangoli,[15] K. A. Zarebski,[47] M. Zavertyaev,[11,w] L. Zhang,[3] Y. Zhang,[7] Y. Zhang,[63] A. Zhelezov,[12] Y. Zheng,[63] A. Zhokhov,[32] X. Zhu,[3] V. Zhukov,[9] and S. Zucchelli[15]

(LHCb Collaboration)

[1]*Centro Brasileiro de Pesquisas Físicas (CBPF), Rio de Janeiro, Brazil*
[2]*Universidade Federal do Rio de Janeiro (UFRJ), Rio de Janeiro, Brazil*
[3]*Center for High Energy Physics, Tsinghua University, Beijing, China*
[4]*LAPP, Université Savoie Mont-Blanc, CNRS/IN2P3, Annecy-Le-Vieux, France*
[5]*Clermont Université, Université Blaise Pascal, CNRS/IN2P3, LPC, Clermont-Ferrand, France*
[6]*CPPM, Aix-Marseille Université, CNRS/IN2P3, Marseille, France*
[7]*LAL, Université Paris-Sud, CNRS/IN2P3, Orsay, France*
[8]*LPNHE, Université Pierre et Marie Curie, Université Paris Diderot, CNRS/IN2P3, Paris, France*
[9]*I. Physikalisches Institut, RWTH Aachen University, Aachen, Germany*
[10]*Fakultät Physik, Technische Universität Dortmund, Dortmund, Germany*
[11]*Max-Planck-Institut für Kernphysik (MPIK), Heidelberg, Germany*
[12]*Physikalisches Institut, Ruprecht-Karls-Universität Heidelberg, Heidelberg, Germany*
[13]*School of Physics, University College Dublin, Dublin, Ireland*
[14]*Sezione INFN di Bari, Bari, Italy*
[15]*Sezione INFN di Bologna, Bologna, Italy*
[16]*Sezione INFN di Cagliari, Cagliari, Italy*
[17]*Sezione INFN di Ferrara, Ferrara, Italy*

[18]*Sezione INFN di Firenze, Firenze, Italy*
[19]*Laboratori Nazionali dell'INFN di Frascati, Frascati, Italy*
[20]*Sezione INFN di Genova, Genova, Italy*
[21]*Sezione INFN di Milano Bicocca, Milano, Italy*
[22]*Sezione INFN di Milano, Milano, Italy*
[23]*Sezione INFN di Padova, Padova, Italy*
[24]*Sezione INFN di Pisa, Pisa, Italy*
[25]*Sezione INFN di Roma Tor Vergata, Roma, Italy*
[26]*Sezione INFN di Roma La Sapienza, Roma, Italy*
[27]*Henryk Niewodniczanski Institute of Nuclear Physics Polish Academy of Sciences, Kraków, Poland*
[28]*AGH - University of Science and Technology, Faculty of Physics and Applied Computer Science, Kraków, Poland*
[29]*National Center for Nuclear Research (NCBJ), Warsaw, Poland*
[30]*Horia Hulubei National Institute of Physics and Nuclear Engineering, Bucharest-Magurele, Romania*
[31]*Petersburg Nuclear Physics Institute (PNPI), Gatchina, Russia*
[32]*Institute of Theoretical and Experimental Physics (ITEP), Moscow, Russia*
[33]*Institute of Nuclear Physics, Moscow State University (SINP MSU), Moscow, Russia*
[34]*Institute for Nuclear Research of the Russian Academy of Sciences (INR RAN), Moscow, Russia*
[35]*Yandex School of Data Analysis, Moscow, Russia*
[36]*Budker Institute of Nuclear Physics (SB RAS), Novosibirsk, Russia*
[37]*Institute for High Energy Physics (IHEP), Protvino, Russia*
[38]*ICCUB, Universitat de Barcelona, Barcelona, Spain*
[39]*Universidad de Santiago de Compostela, Santiago de Compostela, Spain*
[40]*European Organization for Nuclear Research (CERN), Geneva, Switzerland*
[41]*Institute of Physics, Ecole Polytechnique Fédérale de Lausanne (EPFL), Lausanne, Switzerland*
[42]*Physik-Institut, Universität Zürich, Zürich, Switzerland*
[43]*Nikhef National Institute for Subatomic Physics, Amsterdam, The Netherlands*
[44]*Nikhef National Institute for Subatomic Physics and VU University Amsterdam, Amsterdam, The Netherlands*
[45]*NSC Kharkiv Institute of Physics and Technology (NSC KIPT), Kharkiv, Ukraine*
[46]*Institute for Nuclear Research of the National Academy of Sciences (KINR), Kyiv, Ukraine*
[47]*University of Birmingham, Birmingham, United Kingdom*
[48]*H.H. Wills Physics Laboratory, University of Bristol, Bristol, United Kingdom*
[49]*Cavendish Laboratory, University of Cambridge, Cambridge, United Kingdom*
[50]*Department of Physics, University of Warwick, Coventry, United Kingdom*
[51]*STFC Rutherford Appleton Laboratory, Didcot, United Kingdom*
[52]*School of Physics and Astronomy, University of Edinburgh, Edinburgh, United Kingdom*
[53]*School of Physics and Astronomy, University of Glasgow, Glasgow, United Kingdom*
[54]*Oliver Lodge Laboratory, University of Liverpool, Liverpool, United Kingdom*
[55]*Imperial College London, London, United Kingdom*
[56]*School of Physics and Astronomy, University of Manchester, Manchester, United Kingdom*
[57]*Department of Physics, University of Oxford, Oxford, United Kingdom*
[58]*Massachusetts Institute of Technology, Cambridge, MA, United States*
[59]*University of Cincinnati, Cincinnati, OH, United States*
[60]*University of Maryland, College Park, MD, United States*
[61]*Syracuse University, Syracuse, NY, United States*
[62]*Pontifícia Universidade Católica do Rio de Janeiro (PUC-Rio), Rio de Janeiro, Brazil (associated with Institution Universidade Federal do Rio de Janeiro (UFRJ), Rio de Janeiro, Brazil)*
[63]*University of Chinese Academy of Sciences, Beijing, China (associated with Institution Center for High Energy Physics, Tsinghua University, Beijing, China)*
[64]*Institute of Particle Physics, Central China Normal University, Wuhan, Hubei, China (associated with Institution Center for High Energy Physics, Tsinghua University, Beijing, China)*
[65]*Departamento de Fisica , Universidad Nacional de Colombia, Bogota, Colombia (associated with Institution LPNHE, Université Pierre et Marie Curie, Université Paris Diderot, CNRS/IN2P3, Paris, France)*
[66]*Institut für Physik, Universität Rostock, Rostock, Germany (associated with Institution Physikalisches Institut, Ruprecht-Karls-Universität Heidelberg, Heidelberg, Germany)*
[67]*National Research Centre Kurchatov Institute, Moscow, Russia (associated with Institution Institute of Theoretical and Experimental Physics (ITEP), Moscow, Russia)*

[68]*Instituto de Fisica Corpuscular (IFIC), Universitat de Valencia-CSIC, Valencia, Spain (associated with Institution ICCUB, Universitat de Barcelona, Barcelona, Spain)*
[69]*Van Swinderen Institute, University of Groningen, Groningen, The Netherlands (associated with Institution Nikhef National Institute for Subatomic Physics, Amsterdam, The Netherlands)*

[a]Also at Università di Ferrara, Ferrara, Italy.
[b]Also at Università di Milano Bicocca, Milano, Italy.
[c]Also at Università di Modena e Reggio Emilia, Modena, Italy.
[d]Also at Novosibirsk State University, Novosibirsk, Russia.
[e]Also at LIFAELS, La Salle, Universitat Ramon Llull, Barcelona, Spain.
[f]Also at Università di Bologna, Bologna, Italy.
[g]Also at Università di Roma Tor Vergata, Roma, Italy.
[h]Also at Università di Genova, Genova, Italy.
[i]Also at Scuola Normale Superiore, Pisa, Italy.
[j]Also at Università di Cagliari, Cagliari, Italy.
[k]Also at Università di Padova, Padova, Italy.
[l]Also at Università di Bari, Bari, Italy.
[m]Also at Laboratoire Leprince-Ringuet, Palaiseau, France.
[n]Also at Università degli Studi di Milano, Milano, Italy.
[o]Also at Universidade Federal do Triângulo Mineiro (UFTM), Uberaba-MG, Brazil.
[p]Also at AGH - University of Science and Technology, Faculty of Computer Science, Electronics and Telecommunications, Kraków, Poland.
[q]Also at Iligan Institute of Technology (IIT), Iligan, Philippines.
[r]Also at Hanoi University of Science, Hanoi, Viet Nam.
[s]Also at Università di Pisa, Pisa, Italy.
[t]Also at Università di Roma La Sapienza, Roma, Italy.
[u]Also at Università della Basilicata, Potenza, Italy.
[v]Also at Università di Urbino, Urbino, Italy.
[w]Also at P.N. Lebedev Physical Institute, Russian Academy of Science (LPI RAS), Moscow, Russia.